Self-radiolysis of tritiated water. 3. The (OH)-O-center dot scavenging effect of bromide ions on the yield of H2O2 in the radiolysis of water by Co-60 gamma-rays and tritium beta-...

ARTICLE *in* RSC ADVANCES · SEPTEMBER 2014

Impact Factor: 3.84 · DOI: 10.1039/C4RA06707J

6 AUTHORS, INCLUDING:

Shayla Mustaree
Université de Sherbrooke
1 PUBLICATION **3** CITATIONS
SEE PROFILE

Sofia Loren Butarbutar
Badan Tenaga Nuklir Nasional
7 PUBLICATIONS **5** CITATIONS
SEE PROFILE

Craig R Stuart
Canadian Nuclear Laboratories
12 PUBLICATIONS **513** CITATIONS
SEE PROFILE

RSC Advances

PAPER

View Article Online
View Journal | View Issue

Cite this: *RSC Adv.*, 2014, **4**, 43572

Self-radiolysis of tritiated water. 3. The ˙OH scavenging effect of bromide ions on the yield of H_2O_2 in the radiolysis of water by ^{60}Co γ-rays and tritium β-particles at room temperature

Shayla Mustaree,[a] Jintana Meesungnoen,[a] Sofia Loren Butarbutar,[ab] Patrick Causey,[c] Craig R. Stuart[c] and Jean-Paul Jay-Gerin*[a]

Monte Carlo track chemistry simulations were used to determine the yields (or *G*-values) of hydrogen peroxide in the radiolysis of neutral water and dilute aqueous bromide solutions by low linear energy transfer (LET ∼ 0.3 keV μm^{-1}) radiation (*e.g.*, γ-rays from ^{60}Co, fast electrons or high-energy protons) and tritium β-particles (mean LET ∼ 6 keV μm^{-1}) at 25 °C. We investigated the influence of Br^- ions, as selective scavengers of ˙OH radical precursors of H_2O_2, on the inhibition of $G(H_2O_2)$ for these two types of radiation. Studying this system under a wide range of Br^- concentrations (5×10^{-7} to 0.2 M) and using a well-accepted mechanism for radiolysis in the presence or absence of air, we examined the chemical changes in the scavengeability of H_2O_2 produced by 300 MeV irradiating protons (used in this work to reproduce the effects of ^{60}Co γ/fast electron radiolysis) and tritium β-electron radiolysis. We found that these changes could be related to differences in the initial spatial distributions of radiolytic species (*i.e.*, the structure of the electron tracks, the low-energy β-electrons of tritium depositing their energy almost entirely as cylindrical "short tracks" and the energetic Compton electrons produced by γ-radiolysis forming mainly spherical "spurs"), in full agreement with previous experimental and theoretical work. Simulations showed that the short track geometry of higher LET tritium β-electrons in both water and aqueous bromide solutions favored a clear increase in $G(H_2O_2)$ compared to ^{60}Co γ-rays. Moreover, the presence of oxygen was seen to scavenge hydrated electrons (e_{aq}^-) and H˙ atoms on the ∼10^{-7} s time scale, thereby protecting H_2O_2 from further reactions with these species in the homogeneous stage of radiolysis. This protection against e_{aq}^- and H˙ atoms therefore led to an increase in the long time H_2O_2 yields, as seen experimentally. Finally, for both deaerated and aerated solutions, the H_2O_2 yield in tritium β-radiolysis was found to be more easily suppressed than in the case of cobalt γ-radiolysis, and interpreted by the quantitatively different chemistry between spurs and short tracks. These differences in the scavengeability of H_2O_2 precursors in passing from 300 MeV irradiating protons to tritium β-electron irradiation were in good agreement with experimental data, thereby lending strong support to the picture of tritium β-radiolysis in terms of short tracks of high local LET.

Received 6th July 2014
Accepted 1st September 2014

DOI: 10.1039/c4ra06707j

www.rsc.org/advances

1. Introduction

In the study of the radiation chemistry of water, the main goal is to determine the yields (or *G*-values) of the radicals and molecules produced by the irradiation. In the case of low "linear energy transfer" (LET), sparsely ionizing radiation (*e.g.*, energetic photons, such as γ-rays from ^{60}Co or ^{137}Cs or hard X-rays, or high-energy charged particles, such as fast electrons or high-energy protons generated by a particle accelerator), each energy-transfer event of a fast electron produces a cluster of reactive species, commonly known as a spur.[1,2] Under conventional irradiation conditions (*i.e.*, at modest dose rates so that no track overlap occurs), these species are generated nonhomogeneously on subpicosecond time scales[3] along the track of the incident radiation[4] and include the hydrated electron (e_{aq}^-), H^+, H˙, ˙OH, H_2, H_2O_2, OH^-, $O_2^{\cdot -}$ [or its protonated form $HO_2^{\cdot}$, depending on the pH; $pK_a(HO_2^{\cdot}/O_2^{\cdot -}) = 4.8$ in water at 25 °C], *etc.*[5–8] As they diffuse away from the site where they were originally produced, these species either react within the spurs as they develop in

[a]*Département de médecine nucléaire et de radiobiologie, Faculté de médecine et des sciences de la santé, Université de Sherbrooke, 12e Avenue Nord, Sherbrooke (Québec), J1H 5N4, Canada. E-mail: jean-paul.jay-gerin@USherbrooke.ca; Fax: +1 819 564 5442; Tel: +1 819 346 1110 ext. 14682/14773*

[b]*Center for Reactor Technology and Nuclear Safety, National Nuclear Energy Agency, Puspiptek Area, Serpong, Tangerang Selatan, Banten 15314, Indonesia*

[c]*Chalk River Laboratories, Reactor Chemistry and Corrosion Branch, Atomic Energy of Canada Limited, Chalk River (Ontario), K0J 1J0, Canada. E-mail: causeyp@aecl.ca; stuartc@aecl.ca; Fax: +1 613 584 8219; Tel: +1 613 584 8811 ext. 44018/43380*

time or escape into the bulk solution. At ambient temperature and pressure, the so-called "spur expansion" is essentially complete by ~0.2 μs after the initial energy deposition.[9] At this time, the species that have escaped from spur reactions become homogeneously distributed throughout the bulk of the solution (also referred to as the "background") and the track of the radiation no longer exists.[10] The radical and molecular products, considered as additions to the background, are then available for reaction with dissolved solutes (if any) present (in low or moderate concentrations) at the time of irradiation.

Compared to the chemical effects of ^{60}Co γ-radiolysis, which are mainly due to Compton electrons with an initial energy of about 1 MeV, the chemistry of water and aqueous solutions is very different after irradiation with the low-energy β-electrons (~18.6 keV maximum) emitted by tritium (^{3}H).[11,12] This difference reflects the influence of the electron energy on the initial spatial distribution of all the radiolytic species and free radical intermediates (*i.e.*, the electron track structure) created in the two cases;[13–16] primary events are more well-separated in the tracks of higher-energy electrons.[16–18] Fig. 1 illustrates typical two-dimensional representations of the track segment of a 300 MeV irradiating proton (panel a) and the complete track of an incident 7.8 keV ^{3}H β-electron (ref. 19) (panel b), calculated with our IONLYS Monte Carlo simulation code (see below). Fig. 1, panel c, shows, for the sake of comparison, the simulated track history of a 150 keV incident electron.[16] As can be seen, the initial distributions of the energy deposition for ~300 MeV protons and ~150 keV electrons are quite similar, indicating that they have the same mean LET. This similarity clearly supports the validity of our choice of using short-track segments of ~300 MeV incident protons of well-defined LET (~0.3 keV μm^{-1}) in our simulations to reproduce the effects of ^{60}Co γ/fast electron radiolysis.[8,18] Using the terminology of the Mozumder–Magee model of energy deposition,[4,20] while fast electrons predominantly form "spurs" (spherical geometry), the low-energy β-electrons of tritium predominantly deposit energy in "short tracks" (columnar geometry); this leads to an increased amount of intra-track chemistry. The short-track geometry favors radical–radical reactions in the diffusing tracks, which increases the proportion of molecular products at the expense of the radical products.

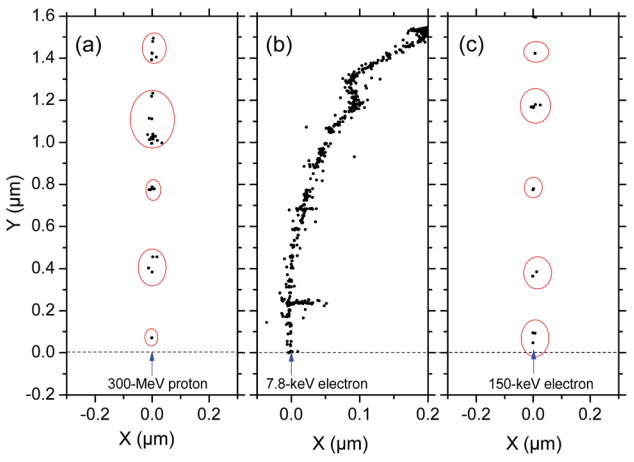

Fig. 1 Simulated track histories (at ~10^{-13} s, projected into the *XY* plane of figure) of a 300 MeV proton (panel a), a 7.8 keV ^{3}H β-electron (panel b), and a 150 keV electron (panel c) incident on liquid water at 25 °C. Panel c shows the similarity of the track structures of a 150 keV incident electron and of a 300 MeV irradiating proton (panel a). The three irradiating particles are generated at the origin and start traveling along the *Y* axis. Dots represent the energy deposited at points where an interaction occurred.

In the work presented in this paper, an attempt is made to further distinguish the properties of spurs and short tracks by examining the differences in scavengeability of the hydrogen peroxide yield produced after irradiation with ~300 MeV incident protons (which mimic ^{60}Co γ-ray or fast electron irradiation) and by tritium β-radiolysis.[14,15,21,22]

Molecular H_2O_2 is one of the main oxidizing species formed in the radiolysis of water, and its yield is of interest to studies of many aspects of fundamental and applied radiation effects.[23] No real-time studies on H_2O_2 formation have been performed and its temporal dependence is usually probed by varying the concentration of appropriate scavengers for the $^{\bullet}$OH radical. Bromide anions are used in this study as selective scavengers of the $^{\bullet}$OH radical precursors of H_2O_2. Our primary purpose is twofold: (a) to compare the effect of Br^- concentration on the yield of H_2O_2, $G(H_2O_2)$, produced by the two types of radiation studied in aqueous solutions at neutral pH using Monte Carlo track chemistry simulations in conjunction with available experimental data, and (b) to relate the different H_2O_2 scavengeabilities found to differences in the initial spatial distribution of radiolytic species (*i.e.*, the structure of the radiation track) in the two cases.

2. Radiolysis of (dilute) aqueous Br^- scavenger solutions

The Br^- ion is inert toward e_{aq}^-, reacts slowly with H$^{\bullet}$ atoms, but it reacts very efficiently with $^{\bullet}$OH radicals. The mechanism of its action, which has been the subject of many radiation chemistry studies in the past,[24–35] is relatively well understood and the rate constants at 25 °C of the relevant reactions are known. Pulse radiolysis has shown that the reaction of $^{\bullet}$OH with Br^- takes place through the formation of the intermediate adduct $BrOH^{\bullet -}$,[36] which then transforms to Br$^{\bullet}$, $Br_2^{\bullet -}$ and other bromine species. Table 1 provides a numbered list of reactions and corresponding rate constants used in this work. Whereas the mechanism of radiolytic oxidation of Br^- by $^{\bullet}$OH radicals is quite complex, the major fast kinetic steps in dilute aqueous bromide solutions are dominated by the sequence of (reversible) reactions (R1–R5).[36–39]

Besides the scavenging intervention of bromide ions, the decay of $^{\bullet}$OH radicals also involves reactions mainly with the radical species e_{aq}^-, $^{\bullet}$OH, and H$^{\bullet}$ that are formed in the water of the irradiated solutions:

$$^{\bullet}OH + e_{aq}^- \rightarrow OH^- \; k_1 = 3.5 \times 10^{10}\ M^{-1}\ s^{-1} \quad (1)$$

$$^{\bullet}OH + {}^{\bullet}OH \rightarrow H_2O_2 \; k_2 = 6.3 \times 10^{9}\ M^{-1}\ s^{-1} \quad (2)$$

Table 1 Reactions and rate constants (k) used for modeling the radiolytic oxidation of Br^- by $^{\bullet}OH$ radicals in aqueous solutions at 25 °C. For first-order reactions (indicated by the symbol §), the value of k is given in s^{-1}. Note that the rate constants given here for the reactions between ions are in the limit of zero ionic strength (*i.e.*, at infinite dilution of ions)

	Reaction	k (M^{-1} s^{-1})
R1	$^{\bullet}OH + Br^- \rightarrow BrOH^{\bullet -}$	1.1×10^{10}
R2	$BrOH^{\bullet -} + H^+ \rightarrow Br^{\bullet} (+H_2O)$	4.4×10^{10}
R3	$BrOH^{\bullet -} \rightarrow Br^{\bullet} + OH^-$	4.2×10^{6}§
R4	$BrOH^{\bullet -} + Br^- \rightarrow Br_2^{\bullet -} + OH^-$	1.9×10^{8}
R5	$Br^{\bullet} + Br^- \rightarrow Br_2^{\bullet -}$	1.2×10^{10}
R6	$BrOH^{\bullet -} \rightarrow {}^{\bullet}OH + Br^-$	3.3×10^{7}§
R7	$Br^{\bullet} (+H_2O) \rightarrow BrOH^{\bullet -} + H^+$	1.4§
R8	$Br^{\bullet} + OH^- \rightarrow BrOH^{\bullet -}$	1.3×10^{10}
R9	$Br_2^{\bullet -} + OH^- \rightarrow BrOH^{\bullet -} + Br^-$	2.7×10^{6}
R10	$Br_2^{\bullet -} \rightarrow Br^{\bullet} + Br^-$	1.9×10^{4}§
R11	$Br_2^{\bullet -} + Br_2^{\bullet -} \rightarrow Br_3^- + Br^-$	2.4×10^{9}
R12	$Br^{\bullet} + Br_2^{\bullet -} \rightarrow Br_3^-$	5×10^{9}
R13	$Br^- + Br_2 \rightarrow Br_3^-$	1.6×10^{8}
R14	$Br_3^- \rightarrow Br^- + Br_2$	10^{7}§
R15	$Br^{\bullet} + Br^{\bullet} \rightarrow Br_2$	5×10^{9}
R16	$Br^{\bullet} + e_{aq}^- \rightarrow Br^-$	10^{10}
R17	$Br_2 + e_{aq}^- \rightarrow Br^{\bullet} + Br^-$	4.2×10^{10}
R18	$Br_2^{\bullet -} + e_{aq}^- \rightarrow 2Br^-$	1.3×10^{10}
R19	$Br_3^- + e_{aq}^- \rightarrow Br^- + Br_2^{\bullet -}$	2.7×10^{10}
R20	$Br^{\bullet} + H^{\bullet} \rightarrow Br^- + H^+$	10^{10}
R21	$Br^- + H^{\bullet} \rightarrow HBr^{\bullet -}$	1.7×10^{6}
R22	$HBr^{\bullet -} + H^+ \rightarrow H_2 + Br^{\bullet}$	1.1×10^{10}
R23	$Br_2 + H^{\bullet} \rightarrow Br^{\bullet} + Br^- + H^+$	4.2×10^{10}
R24	$Br_2^{\bullet -} + H^{\bullet} \rightarrow 2Br^- + H^+$	1.4×10^{10}
R25	$Br_3^- + H^{\bullet} \rightarrow Br^- + Br_2^{\bullet -} + H^+$	1.2×10^{10}
R26	$Br_2^{\bullet -} + H_2O_2 \rightarrow HO_2^{\bullet} + 2Br^- + H^+$	10^{3}
R27	$Br^{\bullet} + HO_2^{\bullet} \rightarrow Br^- + O_2 + H^+$	1.6×10^{8}
R28	$Br_2 + HO_2^{\bullet} \rightarrow Br^{\bullet} + Br^- + O_2 + H^+$	1.5×10^{8}
R29	$Br_2^{\bullet -} + HO_2^{\bullet} \rightarrow 2Br^- + O_2 + H^+$	10^{8}
R30	$Br_3^- + HO_2^{\bullet} \rightarrow Br^- + Br_2^{\bullet -} + O_2 + H^+$	10^{7}
R31	$Br_2^{\bullet -} + O_2^{\bullet -} \rightarrow 2Br^- + O_2$	1.7×10^{8}
R32	$Br_3^- + O_2^{\bullet -} \rightarrow Br^- + Br_2^{\bullet -} + O_2$	1.5×10^{9}

$$^{\bullet}OH + H^{\bullet} \rightarrow H_2O \; k_3 = 1.6 \times 10^{10}\ M^{-1}\ s^{-1}, \quad (3)$$

which are listed here in order of importance at 25 °C.[16,40] Because reaction (2) is the primary mechanism to form the molecular product H_2O_2,[41,42] the presence of Br^- ions can therefore lower the radiolytic formation of hydrogen peroxide through the competition of reaction (R1).

In the presence of air or oxygen, e_{aq}^- and $H^{\bullet}$ are converted to $O_2^{\bullet -}$ and $HO_2^{\bullet}$, respectively, according to[16,43]

$$e_{aq}^- + O_2 \rightarrow O_2^{\bullet -} \; k_4 = 2.3 \times 10^{10}\ M^{-1}\ s^{-1} \quad (4)$$

$$H^{\bullet} + O_2 \rightarrow HO_2^{\bullet} \; k_5 = 1.3 \times 10^{10}\ M^{-1}\ s^{-1}. \quad (5)$$

The hydroperoxyl/superoxide ($HO_2^{\bullet}/O_2^{\bullet -}$) radicals so formed either combine to form H_2O_2 according to[16,44]

$$HO_2^{\bullet} + HO_2^{\bullet} \rightarrow H_2O_2 + O_2 \; k_6 = 8.4 \times 10^{5}\ M^{-1}\ s^{-1} \quad (6)$$

$$HO_2^{\bullet} + O_2^{\bullet -} \rightarrow HO_2^- + O_2 \; k_7 = 9.7 \times 10^{7}\ M^{-1}\ s^{-1}, \quad (7)$$

react with $^{\bullet}OH$ radicals according to

$$HO_2^{\bullet} + {}^{\bullet}OH \rightarrow O_2 + H_2O \; k_8 = 6.6 \times 10^{9}\ M^{-1}\ s^{-1} \quad (8)$$

$$O_2^{\bullet -} + {}^{\bullet}OH \rightarrow O_2 + OH^- \; k_9 = 7 \times 10^{9}\ M^{-1}\ s^{-1} \quad (9)$$

or are scavenged by secondary products such as $Br^{\bullet}$, Br_2, $Br_2^{\bullet -}$ and Br_3^- according to reactions (R27–R32).

3. Monte Carlo track structure/chemistry simulations

To help assess the basic molecular processes that are involved in the mechanism of action of Br^- ions, a full Monte Carlo computer code, called IONLYS-IRT,[8] has been used to simulate in detail the radiolysis of the studied aqueous bromide solutions. Indeed, Monte Carlo simulation methods are well suited to take into account the stochastic nature of the complex sequence of events that are generated in these solutions after absorption of ionization radiation. The simulation allows the reconstruction of the intricate action of the radiation, thus providing a powerful tool for studying the relationship between the initial radiation track structure, the ensuing chemical processes, and the stable end products formed by radiolysis. Since a detailed description of our Monte Carlo approach for fast electron and proton track structures in both pure water and water-containing solutes at ambient temperature and the "independent reaction times" (IRT) simulation method used to model the subsequent nonhomogeneous/homogeneous chemistry have been given previously,[8,16,41,45–50] only a brief overview of the most essential features of our code is given below.

The IONLYS step-by-step simulation program covers the early physical and physicochemical stages of radiation action up to ~1 ps in the track development. It is composed of two modules: one is for transporting the incident charged particle investigated (called either TRACEPR for an impacting primary electron or TRACPRO for an incident proton), and the other (called TRACELE) is for transporting all of the energetic (or "dry") electrons (collectively named "secondary electrons") resulting from the ionization of the water molecules until they become "thermalized" and subsequently "trapped" and "hydrated".[16,45] The TRACEPR module of IONLYS was used in this study to simulate the radiolysis of bromide solutions by the tritium-decay β-electrons. As for the TRACPRO module, it was used here to simulate track segments of ~300 MeV incident protons (LET ~0.3 keV μm^{-1} at 25 °C).

The complex spatial distribution of reactants at the end of the physicochemical stage, which is provided as an output of the IONLYS (TRACELE) program, is then directly used as the starting point for the subsequent "nonhomogeneous" chemical stage. This stage, during which the different species diffuse randomly at rates determined by their diffusion coefficients and react with, or compete with, one another as well as with any added solutes present at the time of irradiation until all spur/track reactions are complete (typically, on the time scale from ~1 ps to ~0.1–1 μs at room temperature), is covered by our IRT program. This program employs the IRT method, a computer-

efficient stochastic simulation technique that is used to simulate reaction times without having to follow the trajectories of the diffusing species.[51,52] Its implementation has been described in detail previously,[41] and its ability to give accurate time-dependent chemical yields over a wide range of irradiation conditions has been well validated by comparison with full random flight (or step-by-step) Monte Carlo simulations, which do follow the reactant trajectories in detail.[53,54] This IRT program can also be used to efficiently describe the evolution of radiation-induced yields in the "homogeneous" chemical stage that takes place at longer time scales.[16,48–50,55]

The reaction scheme for the radiolysis of pure liquid water used in IONLYS-IRT is the same as used previously (see Table 1 of ref. 16). Values of the diffusion coefficients of the reactive species involved in the simulations are listed in Table 6 of ref. 56. The effects of dissolved Br^- ions on the radiolysis yields have been modeled by incorporating the 32 chemical reactions listed in Table 1, which account for the species $Br^\bullet$, Br_2, $Br_2^{\bullet-}$, Br_3^-, and $BrOH^{\bullet-}$ present in irradiated solutions under aerated or deaerated conditions. The diffusion coefficients used for Br^- and for these bromine species are 2.1, 2.1, 1.1, 1.2, 1.1, and 1.1 $\times$ 10^{-5} cm^2 s^{-1}, respectively.[38,57]

In addition, we have introduced in the IRT program the effect of ionic strength of the solutions on all reactions between ions. The correction to the reaction rate constants was made as described in ref. 49 and 58. Finally, in our simulations, the "direct" ionization of Br^- (to give e_{aq}^- and $Br^\bullet$) was neglected, which is a reasonably good approximation over the range of Br^- concentrations (5×10^{-7} to 0.2 M) studied here.

Tritium-β primary electron track structures were simulated using the TRACEPR and TRACELE modules of IONLYS. These programs follow, event-by-event, the spatial and temporal coordinates of the primary electron and all subsequent secondaries in water during the slowing down processes, thus generating the complete physical track structure. Each simulation typically involved ~6000 different whole track histories. This number was chosen so as to ensure only small statistical fluctuations in the computed averages of chemical yields, while keeping acceptable computer time limits. To reproduce the effects of ^{60}Co γ/fast electron radiolysis, we used short (typically ~150 μm) segments of ~300 MeV irradiating proton tracks, over which the average LET value obtained in the simulations was nearly constant and equal to ~0.3 keV μm^{-1} at 25 °C. Such model calculations thus gave track segment yields at a well-defined LET.[41,59] The simulations, performed with the TRACPRO module of IONLYS, consist of following the transport and energy loss of an incident proton until it has penetrated the chosen length of the track segment into the medium. As shown in Fig. 1, due to its large mass, the impacting proton is almost not deflected by collisions with the target electrons.[45,59] The number of proton histories (usually ~150) was chosen to permit averaging of results with acceptable statistical confidence. In the simulations reported here, the time evolution of $G(H_2O_2)$ has been followed until 0.1 ms for all considered concentrations of added bromide in the presence or absence of oxygen.

Throughout this study, we assumed tritiated water concentrations to be low enough so that dose-rate effects could be neglected. In this case of low volumic activity (typically below ~2–5 Ci mL^{-1}), tritiated water can then simply be described as a "dilute" solution of ^{3}HOH in water.[60]

4. Results and discussion

Fig. 2 shows the time evolution of $G(H_2O_2)$ as obtained from our simulations of the radiolysis of both deaerated and aerated neutral pH aqueous bromide solutions by 300 MeV incident protons at 25 °C. For the sake of comparison, available experimental data for ^{60}Co γ/fast electron irradiation[7,23,43,61,62] are also included in the figure. As can be seen, the agreement between the calculated and measured yields is satisfactory. In particular, the decrease in the H_2O_2 yield in solutions containing larger Br^- ion amounts is well reproduced by our simulated values. As discussed above, this decrease in H_2O_2 yield is due to reactions of Br^- with $^\bullet$OH radicals *within the spurs*, *i.e.*, at times less than ~0.2 μs, the lifetime of the spur in the ^{60}Co γ radiolysis of water at 25 °C.[9] This is indeed what is observed for the 10^{-3}, 0.01, and

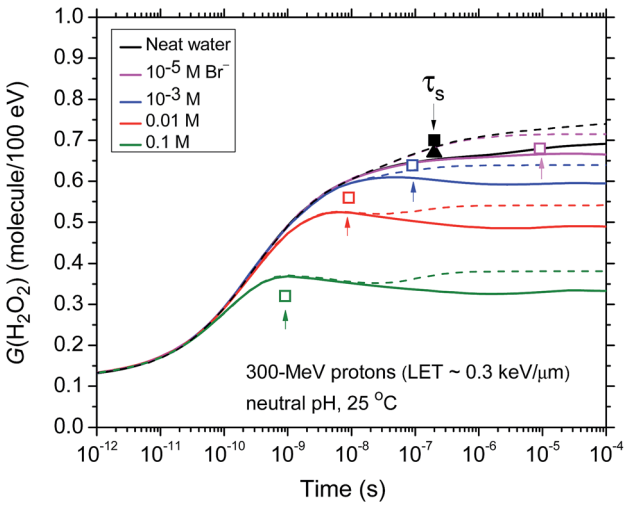

Fig. 2 Time evolution of $G(H_2O_2)$ (in molecule per 100 eV) after 300 MeV proton irradiation (LET ~0.3 keV μm^{-1}) of aqueous bromide solutions at neutral pH and 25 °C, calculated from our Monte Carlo simulations over the interval 10^{-12} to 10^{-4} s. The magenta, blue, red and green lines correspond to four different initial concentrations of bromide ions: 10^{-5}, 10^{-3}, 10^{-2} and 0.1 M, respectively. The solid lines show our simulated results for *deaerated* solutions whereas the dashed lines are for *air-saturated* solutions (the concentration of dissolved oxygen used in the calculations is 2.5×10^{-4} M). The black solid and dashed lines show the kinetics of H_2O_2 formation in bromide-free deaerated and aerated solutions (shown here for the sake of reference), respectively. The experimental primary (or "escape") yield $g(H_2O_2)$ for ^{60}Co γ/fast electron irradiation of pure, air-free liquid water (pH 7) is taken from ref. 7, 23, 43, and 61 (~0.70 ± 0.03 molecule per 100 eV) (■) and from ref. 62 (0.67 ± 0.01 molecule per 100 eV) (▲). Note that these latter data have been positioned at τ_s ~0.2 μs, the time at which spur overlap is complete at 25 °C (ref. 9). The different colored arrows pointing upwards give the times at which the scavenging of $^\bullet$OH by Br^- is occurring for the different considered bromide ion concentrations. The open squares are the H_2O_2 yields measured (in deaerated conditions) in ref. 23 using bromide as the $^\bullet$OH scavenger for the corresponding scavenging powers (see ref. 63) (*i.e.*, ~10^5, 10^7, 10^8, and 10^9 s^{-1}, respectively).

0.1 M bromide solutions considered in Fig. 2, for which the lifetimes[63] of the $^{\bullet}OH$ radical with respect to reaction (R1) are 0.9×10^{-7}, 0.9×10^{-8}, and 0.9×10^{-9} s, respectively. At lower Br^- ion concentrations, which are equivalent to longer $^{\bullet}OH$ scavenging times[63] in the stage of homogeneous chemistry in the system, reaction (R1) competes less favorably with the combination reaction of $^{\bullet}OH$ radicals, resulting in an increase in H_2O_2 formation. For instance, at 10^{-5} M bromide concentration, the H_2O_2 yield continuously increases with time, reaching a plateau region near 0.68 molecule per 100 eV at 0.9×10^{-5} s, a value that closely approaches the primary (or "escape") yield of H_2O_2 for ^{60}Co γ/fast electron irradiation of pure, air-free liquid water.[7,23,43,61,62]

In Fig. 2, at the considered 10^{-3}, 0.01, and 0.1 M Br^- ion concentrations, the yields of H_2O_2 in deaerated solutions pass through a maximum at the corresponding scavenging times for the $^{\bullet}OH$ radical and then decrease at longer times. This decrease in $G(H_2O_2)$ at long times is due to H_2O_2 being attacked by the hydrated electrons and, but to a lesser extent, $H^{\bullet}$ atoms escaping the spurs, according to the reactions:

$$H_2O_2 + e_{aq}^- \rightarrow {}^{\bullet}OH + OH^- \; k_{10} = 1.1 \times 10^{10}\ M^{-1}\ s^{-1} \quad (10)$$

$$H_2O_2 + H^{\bullet} \rightarrow {}^{\bullet}OH + H_2O \; k_{11} = 9 \times 10^{7}\ M^{-1}\ s^{-1}. \quad (11)$$

The time dependence of the variations in the cumulative yield of H_2O_2 for the different reactions that contribute to $G(H_2O_2)$ (data not shown here) confirms that the decrease of $G(H_2O_2)$ at long times is predominantly due to reaction (10). This is readily explained by the fact that hydrogen peroxide reacts very rapidly with e_{aq}^-. Reaction (11) is much slower with a rate constant about 3 orders of magnitude lower than for reaction (10). Furthermore, the fact that $H^{\bullet}$ atoms are produced in relatively low yield in the γ-radiolysis of neutral water[5–7,43] and that, unlike the hydrated electrons, they are to some extent scavenged by Br^- according to reaction (R21), also explains why $H^{\bullet}$ atoms do not contribute significantly to the destruction of H_2O_2 at long times.

The results for the yields of H_2O_2 in aerated solutions show that the long time yields are increased compared to those in deaerated solutions. Besides the (slight) additional H_2O_2 production by the combination reactions (6) and (7), the main role of oxygen, here, is to compete with the reactions of e_{aq}^- and $H^{\bullet}$ atoms with H_2O_2, reactions (10) and (11). At the concentration of 2.5×10^{-4} M, O_2 can scavenge e_{aq}^- and $H^{\bullet}$ atoms on the ~0.1 μs time scale, thereby protecting the hydrogen peroxide from further reactions with these species in the homogeneous stage of radiolysis.[23,39] This protection against e_{aq}^- and $H^{\bullet}$ atoms therefore leads to an increase in the long time H_2O_2 yields. Indeed, as can be seen in Fig. 2, the long time yields of H_2O_2 in aerated bromide solutions (as well as in neat water) are ~0.05 molecule per 100 eV higher than in deaerated solutions.

The effect of bromide ion concentrations on the lowering of the yield of H_2O_2 in both deaerated and aerated solutions is further illustrated in Fig. 3. The simulated H_2O_2 yields, taken at the times at which $^{\bullet}OH$ radical scavenging by Br^- is occurring, compare very well with the literature values[23,25,62] for ^{60}Co γ/fast

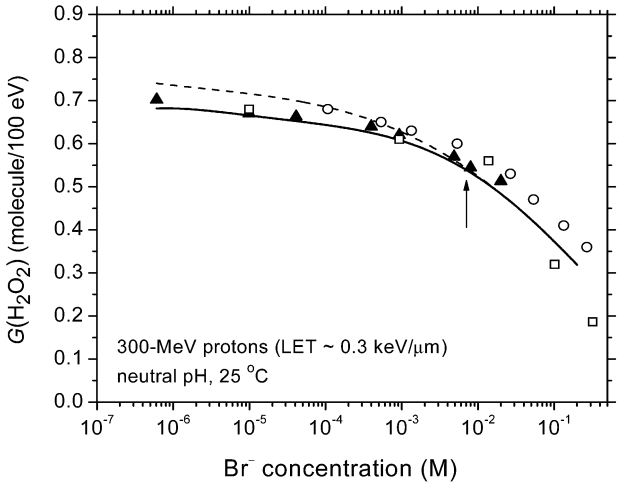

Fig. 3 Decrease in $G(H_2O_2)$ (in molecule per 100 eV) with concentration of Br^- ions for 300 MeV incident protons (LET ~0.3 keV μm^{-1}) in the radiolysis of neutral pH aqueous bromide solutions at 25 °C, calculated from our Monte Carlo simulations over the range of 5×10^{-7} to 0.2 M. Experimental data for ^{60}Co γ/fast electron irradiations: (□) deaerated, ref. 23; (▲) aerated, ref. 25; and (○) deaerated, ref. 62. The solid and dashed lines represent our simulated results of $G(H_2O_2)$, taken at the times at which scavenging of $^{\bullet}OH$ by Br^- is occurring, for deaerated and aerated solutions, respectively. The arrow indicates the Br^- ion concentration (~7×10^{-3} M) below which the scavenging of e_{aq}^- and $H^{\bullet}$ atoms by O_2 in aerated solutions occurs *before* the scavenging of $^{\bullet}OH$ by Br^-.

electron irradiations. At low Br^- ion concentrations (below ~7×10^{-3} M), the scavenging of e_{aq}^- and $H^{\bullet}$ atoms by O_2 in aerated solutions occurs *before* the scavenging of $^{\bullet}OH$ by Br^-. As a result, a larger yield of H_2O_2 is observed compared to the deaerated system, due to the removal of e_{aq}^- and $H^{\bullet}$ atom scavenging of H_2O_2 in reactions (10) and (11). As expected, this effect of dissolved oxygen on the production of H_2O_2 at low bromide concentrations (or, equivalently, under long-time radiolysis conditions) gradually increases as the concentration of Br^- ions decreases toward zero (see Fig. 3).

Fig. 4 shows the kinetics of H_2O_2 formation over the interval ~10^{-12} to 10^{-4} s, as obtained from our Monte Carlo simulations of the radiolysis of both deaerated and aerated neutral pH aqueous bromide solutions by tritium β-particles using 7.8 keV for the initial energy of the β-electrons at 25 °C. It is seen that the variations in $G(H_2O_2)$ at the different Br^- ion concentrations considered are essentially *similar* to those shown in Fig. 2 for 300 MeV incident protons (which, as mentioned earlier, mimic ^{60}Co γ/fast electron irradiation). The simulations show, however, a clear increase (*e.g.*, about 17–25% in neutral water radiolysis) in the absolute value of $G(H_2O_2)$ for ^{3}H β-electrons compared to ^{60}Co γ-rays. Overall, this increase in H_2O_2 yields, when comparing the effects of tritium β-radiolysis with γ-radiolysis, is consistent with differences in the initial spatial distribution of primary transient species (*i.e.*, in the structure of electron tracks).[14,16,18,21] As mentioned earlier, in the "short-track" (columnar) geometry of the higher-LET ^{3}H β-electrons, radicals are formed locally in much higher initial concentration

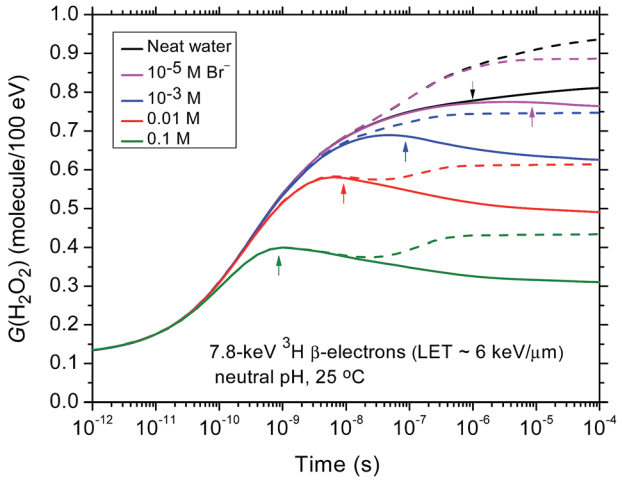

Fig. 4 Time dependence of $G(H_2O_2)$ (in molecule per 100 eV) for the radiolysis of aqueous bromide solutions (pH neutral, 25 °C) by ^{3}H β-particles with initial energy of 7.8 keV (mean energy of energy deposition by the β-particles), calculated from our Monte Carlo simulations over the interval 1 ps–0.1 ms. The magenta, blue, red, and green lines correspond to four different initial concentrations of bromide ions: 10^{-5}, 10^{-3}, 10^{-2}, and 0.1 M, respectively. The solid lines show our simulated results for *deaerated* solutions whereas the dashed lines are for *air-saturated* solutions (the concentration of dissolved oxygen used in the calculations is 2.5×10^{-4} M). The black solid and dashed lines show the kinetics of H_2O_2 formation in bromide-free deaerated and aerated solutions (shown here for the sake of reference), respectively. The different colored arrows pointing upwards give the times at which the scavenging of $^{\bullet}$OH by Br^- is occurring for the different considered bromide ion concentrations. The black arrow pointing downwards indicates our calculated value of the H_2O_2 yield in the 7.8 keV ^{3}H β-electron radiolysis of pure, air-free water at ~1 μs (~0.78 molecule per 100 eV) that we have used in this work for $G^{\circ}(H_2O_2)$ (the yield value obtained by "extrapolating the yields in bromide solutions to zero Br^- concentration") to calculate $G(H_2O_2)$ from the ratios $G(H_2O_2)/G^{\circ}(H_2O_2)$ reported in ref. 22 (see Fig. 5).

than in the spur (spherical) geometry of the energetic Compton electrons of the cobalt-60 γ-rays. As a result, the short-track geometry favors radical–radical reactions in the diffusing tracks, which increases the proportion of molecular products at the expense of the radical products.

Presently, the only data with which we can compare our results are those of Pimblott and LaVerne[18] who investigated the effects of electron energy on the radiolysis of liquid water. Using stochastic track chemistry simulations, these authors calculated the kinetics of formation of H_2O_2 for electrons of initial energy 100 eV to 1 MeV. Remarkably, our H_2O_2 yield obtained for ~7.8 keV ^{3}H β-electrons (~0.75 molecule per 100 eV; see Fig. 4) is in very good agreement with their predicted $G(H_2O_2)$ value at 0.1 μs for deaerated water irradiated by 10 keV incident electrons (0.795 molecule per 100 eV).

As for ~300 MeV irradiating protons (LET ~0.3 keV μm^{-1}) (see Fig. 2), the presence of oxygen is seen to protect, at long times (>10^{-7} s), hydrogen peroxide from the hydrated electrons and H$^{\bullet}$ atoms that escape the tracks. However, as can be seen in Fig. 4, the yields of H_2O_2 at ~0.1 ms in aerated solutions (as well as in neat water) are ~0.12 molecule per 100 eV higher than in deaerated solutions, *i.e.*, about twice as large as what is found in the case of irradiation with 300 MeV incident protons (see Fig. 2). This increase, when comparing the effects of tritium β-radiolysis with ^{60}Co γ/fast electron radiolysis, is related to differences in the structure of electron tracks in the two cases. In the short-track geometry of the higher-LET β-electrons (in contrast with spur geometry), the reactive intermediates are formed in much closer initial proximity, which is favorable to the additional formation of H_2O_2 through the inter-radical $HO_2^{\bullet}/O_2^{\bullet -}$ combination reactions (6) and (7). The effect of dissolved oxygen is thus more pronounced in tritium beta radiolysis, as is seen in Fig. 2 and 4.

The decrease in $G(H_2O_2)$ with concentration of Br^- ions in the ~7.8 keV ^{3}H β-particle radiolysis of both deaerated and aerated neutral pH aqueous bromide solutions at 25 °C, calculated from our Monte Carlo simulations, is shown in Fig. 5. Our calculated yields for deaerated water compare well with the experimental yields of Gagnon and Appleby.[22,64] However, because of the lack of experimental information, no comparison of our simulations could be made for the tritium β-particle radiolysis of aerated solutions. Nevertheless, as for 300 MeV irradiating protons (Fig. 3), the presence of oxygen has an important role in scavenging the hydrated electrons and H$^{\bullet}$ atoms escaping the spur/tracks, and therefore in preventing these species from destroying the hydrogen peroxide at long times (>0.1 μs) *via* the occurrence of reactions (10) and (11). Finally, as discussed above, when comparing the effects of tritium β-radiolysis with γ/fast electron radiolysis, the larger

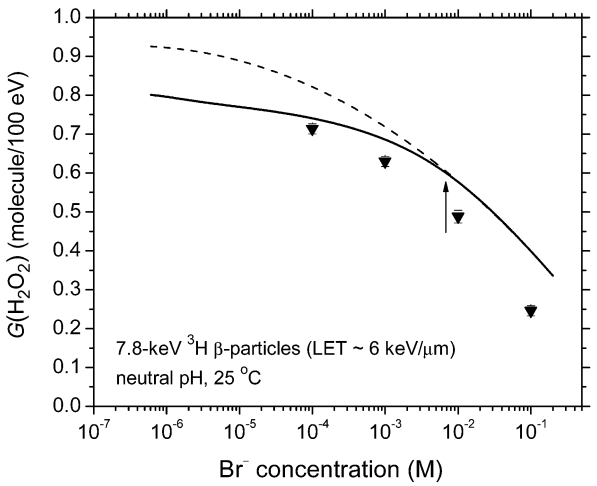

Fig. 5 Decrease in $G(H_2O_2)$ (in molecule per 100 eV) with concentration of Br^- ions for 7.8 keV incident electrons (LET ~6 keV μm^{-1}) in the radiolysis of neutral pH aqueous bromide solutions at 25 °C, calculated from our Monte Carlo simulations over the range of 5×10^{-7} to 0.2 M. The solid and dashed lines represent our simulated results of $G(H_2O_2)$, taken at the times at which scavenging of $^{\bullet}$OH by Br^- is occurring, for deaerated and aerated solutions, respectively. Experimental data for *deaerated* neutral solutions irradiated with tritium β-particles: (▼), Fig. 2 of ref. 22, using $G^{\circ}(H_2O_2) = 0.78$ molecule per 100 eV (see ref. 64 and caption of Fig. 4). The arrow indicates the Br^- ion concentration (~7×10^{-3} M) below which the scavenging of e_{aq}^- and H$^{\bullet}$ atoms by O_2 in aerated solutions occurs *before* the scavenging of $^{\bullet}$OH by Br^-.

H_2O_2 yield difference that is observed at bromide concentrations below $\sim 7 \times 10^{-3}$ M between deaerated and aerated solutions is explained by the chemical differences between spurs and short tracks; the geometry of the short track is more favorable to the inter-radical $HO_2^{\bullet}/O_2^{\bullet-}$ combination reactions (6) and (7), which lead to an additional formation of H_2O_2. This production of H_2O_2 in aerated solutions (*vs.* deaerated solutions) is seen to increase gradually as the concentration of Br^- ions decreases toward zero.

Fig. 6 (panels a and b) shows our calculated results, taken from Fig. 3 and 5, which compare the lowering of $G(H_2O_2)$ formed in the radiolysis of deaerated and aerated bromide solutions (pH 7) by ~300 MeV incident protons and ~7.8 keV ^{3}H β-electrons as a function of Br^- ion concentration over the range of 5×10^{-7} to 0.2 M. For both *air-free* (panel a) and *air-saturated* (panel b) solutions, the H_2O_2 yield in tritium β-radiolysis is more easily suppressed than in the case of ~300 MeV irradiating protons (which mimic irradiation with ^{60}Co γ-rays or fast electrons). These differences in the scavengeability of H_2O_2 precursors are in very good agreement with the experimental data of Gagnon and Appleby,[22] as well as with similar scavenging studies reported by Lemaire *et al.*[14] using bromide and chloride ions as $^{\bullet}OH$ radical scavengers in aerated 0.4 M H_2SO_4 solutions. The fact that it is more difficult to inhibit the yield of H_2O_2 produced by ^{60}Co γ-radiolysis than by the higher-LET tritium β-radiolysis can be interpreted by the chemical differences between spurs and short tracks.[14,22] Briefly, in the short track (cylindrical) geometry, the formation of H_2O_2 takes place over a *longer* time scale as compared with spur (spherical) geometry. Hence, in tritium β-radiolysis, Br^- ions have a longer time scale to react with $^{\bullet}OH$ radicals (the precursors of H_2O_2) than in cobalt γ-radiolysis (which gives predominantly spurs).[15,22] In other words, the molecular H_2O_2 yield formed by tritium β-particles is more scavengeable by Br^- ions than that produced by cobalt γ-rays or fast electrons, as is seen in Fig. 6.

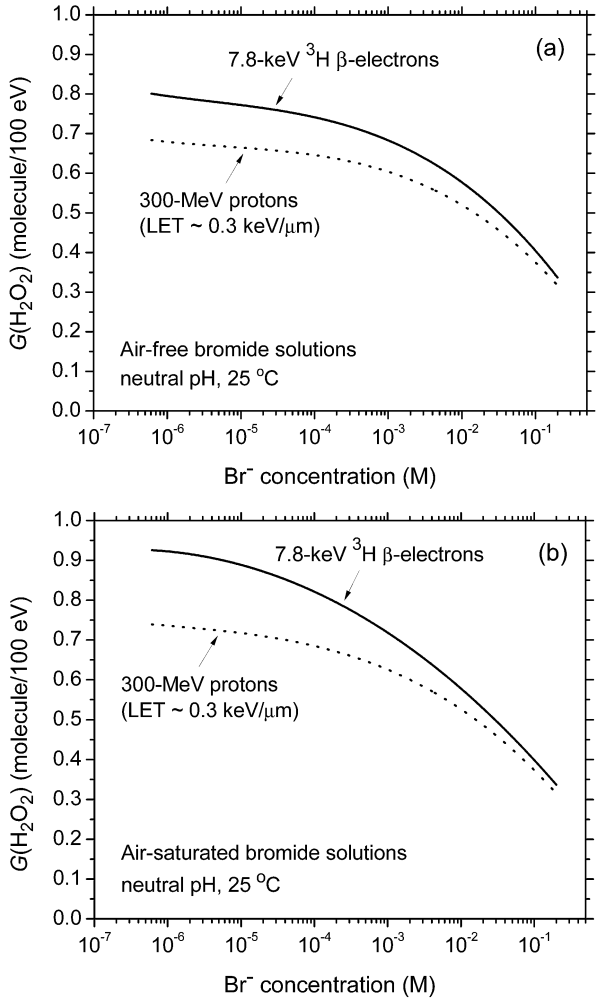

Fig. 6 Inhibition of $G(H_2O_2)$ (in molecule per 100 eV) by bromide ions as obtained from our Monte Carlo simulations of the radiolysis of deaerated (panel a) and aerated (panel b) neutral pH aqueous solutions by ~7.8 keV ^{3}H β-particles (solid lines) and ~300 MeV incident protons (which mimic ^{60}Co γ/fast electron radiolysis) (dotted lines) at 25 °C, as a function of Br^- concentration (data taken from Fig. 3 and 5). In both cases, the inhibition of the H_2O_2 yield for tritium β-rays is greater than for ^{60}Co γ-rays or fast electrons.

5. Conclusions

In this work, Monte Carlo track chemistry simulations have been employed to investigate the $^{\bullet}OH$ scavenging effect of bromide ion on the yield of hydrogen peroxide formation in neutral water irradiated by tritium β-rays and 300 MeV protons (which mimic irradiation with ^{60}Co γ-rays or fast electrons) at 25 °C. The Br^- ion reacts very efficiently with $^{\bullet}OH$ radicals and the mechanism of its action is relatively well understood. Studying this system under a wide range of Br^- concentrations from 5×10^{-7} to 0.2 M, we have examined the differences in the inhibition of H_2O_2 by Br^- ions for the two kinds of radiation considered here. As a general rule, the simulations have clearly shown significant changes in the yields of H_2O_2 in ^{3}H β-particle and cobalt γ/fast electron radiolysis, which have been related to differences in the initial spatial distribution of radiolytic species and free radical intermediates (*i.e.*, the structure of the electron tracks) created in the two cases, in agreement with previous experimental and theoretical work. Indeed, the (cylindrical) short track geometry of higher LET tritium β-electrons in both water and aqueous bromide solutions favors an increased local concentration of reactants and therefore the incidence of an increased amount of intervening intra-track reactions, leading to a clear increase in $G(H_2O_2)$ as compared to γ/fast electron radiolysis (which predominantly gives isolated spherical spurs). For example, as is seen in Fig. 6, our calculated yields of H_2O_2 in deaerated and aerated $\sim 5 \times 10^{-7}$ M bromide solutions (which is the lowest Br^- concentration studied, corresponding to an $^{\bullet}OH$ scavenging time by Br^- of ~0.1 ms) are, respectively, ~17% and ~24% greater in ^{3}H β-particle radiolysis than in high-energy electron/^{60}Co γ-radiolysis.

Furthermore, in aerated bromide solutions ($\sim 2.5 \times 10^{-4}$ M O_2), the presence of oxygen has been seen to scavenge e_{aq}^- and $H^{\bullet}$ atoms on the ~0.1 μs time scale, thereby protecting H_2O_2 from further reactions with these species in the homogeneously distributed bulk of the solution. This protection against e_{aq}^-

and H˙ atoms therefore leads to an increase in the long time H_2O_2 yields, as seen experimentally.

Finally, in the presence and absence of air, the H_2O_2 yield in tritium β-radiolysis is found to be more easily suppressed by Br^- ions than in the case of cobalt γ/fast electron radiolysis. This result can be explained on the same basis due to the quantitatively different chemistry between spurs and short tracks: the time scale for the Br^- ions to react with the ˙OH radicals precursors of H_2O_2 is longer in the short track geometry. These differences in the scavengeability of H_2O_2 precursors in γ- and tritium β-radiolysis agree well with previous experimental data.

In summary, the results of the present simulations lend strong support to the model of tritium β-radiolysis mainly driven by the chemical action of short tracks of high local LET.

Acknowledgements

Financial assistance from Atomic Energy of Canada Limited (Contract no. RD-1.3.5.1-4511) is gratefully acknowledged.

Notes and references

1 A. H. Samuel and J. L. Magee, *J. Chem. Phys.*, 1953, **21**, 1080; J. L. Magee, *Annu. Rev. Nucl. Sci.*, 1953, **3**, 171.

2 G. R. Freeman, in *Proceedings of the Workshop on the Interface between Radiation Chemistry and Radiation Physics, Report ANL-82-88*, ed. M. A. Dillon, R. J. Hanrahan, R. Holroyd, Y.-K. Kim, M. C. Sauer, Jr and L. H. Toburen, Argonne National Laboratory, Argonne, Illinois, 1983, p. 9.

3 R. L. Platzman, in *Radiation Biology and Medicine. Selected Reviews in the Life Sciences*, ed. W. D. Claus, Addison-Wesley, Reading, Massachusetts, 1958, p. 15. See also A. Kuppermann, *J. Chem. Educ.*, 1959, **36**, 279.

4 A. Mozumder, *Fundamentals of Radiation Chemistry*, Academic Press, San Diego, California, 1999.

5 G. V. Buxton, in *Radiation Chemistry: Principles and Applications*, ed. Farhataziz and M. A. J. Rodgers, VCH Publishers, New York, 1987, p. 321.

6 J. W. T. Spinks and R. J. Woods, *An Introduction to Radiation Chemistry*, Wiley, New York, 3rd edn, 1990.

7 C. Ferradini and J.-P. Jay-Gerin, *Can. J. Chem.*, 1999, **77**, 1542.

8 J. Meesungnoen and J.-P. Jay-Gerin, in *Charged Particle and Photon Interactions with Matter. Recent Advances, Applications, and Interfaces*, ed. Y. Hatano, Y. Katsumura and A. Mozumder, Taylor & Francis, Boca Raton, Florida, 2011, p. 355.

9 S. Sanguanmith, J. Meesungnoen, Y. Muroya, M. Lin, Y. Katsumura and J.-P. Jay-Gerin, *Phys. Chem. Chem. Phys.*, 2012, **14**, 16731.

10 Throughout this paper, radiation chemical yields are quoted in units of molecules per 100 eV, as g(X) for primary (or "escape") yields and G(X) for experimentally measured yields. Recall here that the so-called "primary" radical and molecular yields are defined, in the case of low-LET radiation, as the numbers of species formed or destroyed per 100 eV of absorbed energy that remain after "spurs" have dissipated. For conversion into SI units (mol J^{-1}), 1 molecule per 100 eV ≈ 0.10364 μmol J^{-1}

11 Hydrogen-3 or tritium (^{3}H or T) is a radioactive isotope of hydrogen. Its nucleus consists of a proton and two neutrons. The most common chemical form of tritium is tritium oxide, also called "tritiated water" (usually represented as "^{3}HOH"). The chemical properties of tritium are essentially the same as those of ordinary hydrogen. The tritium atom is unstable with a half-life of 12.3 years. As it decays, ^{3}H emits ionizing radiation in the form of β-electrons whose characteristics are: maximum kinetic energy E_{max} ∼ 18.6 keV, average kinetic energy released ∼ 5.7 keV, maximum range in water at 25 °C ∼ 5.5 μm, mean LET in water ∼ 6 keV μm^{-1}

12 D. E. Watt, *Quantities for Dosimetry of Ionizing Radiations in Liquid Water*, Taylor & Francis, London, 1996.

13 A. Appleby and W. F. Gagnon, *J. Phys. Chem.*, 1971, **75**, 601, See also W. F. Gagnon and A. Appleby, *Scavenger studies in tritiated water, Paper of the Journal Series, New Jersey Agricultural Experimental Station*, Rutgers University, Department of Environmental Sciences, New Brunswick, New Jersey, 1971.

14 G. Lemaire, C. Ferradini and J. Pucheault, *J. Phys. Chem.*, 1972, **76**, 1542. See also G. Lemaire and C. Ferradini, *Radiochem. Radioanal. Lett.*, 1970, **5**, 175; G. Lemaire and C. Ferradini, in *Proceedings of the Third Tihany Symposium on Radiation Chemistry*, ed. J. Dobó and P. Hedvig, Akadémiai Kiadó, Budapest, 1972, vol. 2, p. 1213.

15 R. E. Harris and S. M. Pimblott, *Radiat. Res.*, 2002, **158**, 493.

16 L. Mirsaleh Kohan, S. Sanguanmith, J. Meesungnoen, P. Causey, C. R. Stuart and J.-P. Jay-Gerin, *RSC Adv.*, 2013, **3**, 19282.

17 The LET of tritium β-electrons in water (∼6 keV μm^{-1}) is ∼20 times greater than that of the Compton electrons (∼1 MeV) generated by ^{60}Co γ-rays. See, for exampleD. R. McCracken, K. T. Tsang and P. J. Laughton, *Aspects of the physics and chemistry of water radiolysis by fast neutrons and fast electrons in nuclear reactors, Report AECL No. 11895*, Atomic Energy of Canada Limited, Chalk River, Ontario, Canada, 1998. See also I. Plante, A. Filali-Mouhim and J.-P. Jay-Gerin, *Radiat. Phys. Chem.*, 2005, **72**, 173. In this latter article, we developed, for irradiated liquid water, a Java interface software to visualize, in a 3D environment, the spatial distribution of all reactive species present in a radiation track and its subsequent chemical development between ∼1 ps and 1 μs. Examples are given of the chemical evolution of a small portion of a 300 MeV proton track (LET ∼ 0.3 keV μm^{-1}) and of a 5 MeV proton track (LET ∼ 7.9 keV μm^{-1}) (*i.e.*, similar to a 7.8 keV ^{3}H β-electron track whose mean LET in water at room temperature is ∼6 keV μm^{-1}). We refer the reader to this article to have a more direct evidence of the influence of the track structures, in the form of spatial (3D) information as a function of time.

18 S. M. Pimblott and J. A. LaVerne, *Radiat. Res.*, 1998, **150**, 159. Using Monte Carlo track-structure simulations, the authors have shown in this work that the radiation chemistry of

water is unaffected by the *initial* electron energy, E, for 1 MeV > E > 100 keV, which corresponds to the "fast-electron" limit.
19 This electron energy of ~7.8 keV corresponds to the "mean energy of energy deposition" by the β-particles. The use of this single mean "equivalent" electron energy (rather than the commonly used mean of ~5.7 keV) was shown to properly mimic the radiation chemical action of the ^{3}H β-particles and produce representative G-values (ref. 16). See also *ICRU Report 17, Radiation Dosimetry: X Rays Generated at Potentials of 5 to 150 kV*, International Commission on Radiation Units and Measurements, Washington, D.C., 1970.
20 A. Mozumder and J. L. Magee, *Radiat. Res.*, 1966, **28**, 203.
21 E. Collinson, F. S. Dainton and J. Kroh, *Proc. R. Soc. London, Ser. A*, 1962, **265**, 422. See also E. Collinson, F. S. Dainton and J. Kroh, *Proc. R. Soc. London, Ser. A*, 1962, **265**, 430.
22 W. F. Gagnon and A. Appleby, in *Tritium*, ed. A. A. Moghissi and M. W. Carter, Messenger Graphics, Phoenix, Arizona, 1973, p. 192.
23 I. Štefanić and J. A. LaVerne, *J. Phys. Chem. A*, 2002, **106**, 447.
24 T. J. Sworski, *J. Am. Chem. Soc.*, 1954, **76**, 4687.
25 A. O. Allen and R. A. Holroyd, *J. Am. Chem. Soc.*, 1955, **77**, 5852.
26 C. Ferradini and A.-M. Koulkès-Pujo, *J. Chim. Phys.*, 1963, **104**, 1310.
27 B. Čerček, M. Ebert, J. P. Keene and A. J. Swallow, *Science*, 1964, **145**, 919.
28 A. Rafi and H. C. Sutton, *Trans. Faraday Soc.*, 1965, **61**, 877. See also H. C. Sutton, G. E. Adams, J. W. Boag and B. D. Michael, in *Proceedings of the International Symposium on Pulse Radiolysis*, ed. M. Ebert, J. P. Keene, A. J. Swallow and J. H. Baxendale, Academic Press, London, 1965, p. 61.
29 B. Čerček, M. Ebert, C. W. Gilbert and A. J. Swallow, in *Proceedings of the International Symposium on Pulse Radiolysis*, ed. M. Ebert, J. P. Keene, A. J. Swallow and J. H. Baxendale, Academic Press, London, 1965, p. 83.
30 M. S. Matheson, W. A. Mulac, J. L. Weeks and J. Rabani, *J. Phys. Chem.*, 1966, **70**, 2092.
31 Farhataziz, *J. Phys. Chem.*, 1967, **71**, 598.
32 D. Zehavi and J. Rabani, *J. Phys. Chem.*, 1972, **76**, 312.
33 D. Behar, *J. Phys. Chem.*, 1972, **76**, 1815.
34 A. Mamou, J. Rabani and D. Behar, *J. Phys. Chem.*, 1977, **81**, 1447.
35 M. D'Angelantonio, M. Venturi and Q. G. Mulazzani, *Radiat. Phys. Chem.*, 1988, **32**, 319.
36 W. G. Burns and W. R. Marsh, *J. Chem. Soc., Faraday Trans. 1*, 1981, **77**, 197.
37 I. Lampre, J.-L. Marignier, M. Mirdamadi-Esfahani, P. Pernot, P. Archirel and M. Mostafavi, *J. Phys. Chem. A*, 2013, **117**, 877.
38 A. K. El Omar, U. Schmidhammer, A. Balcerzyk, J. A. LaVerne and M. Mostafavi, *J. Phys. Chem. A*, 2013, **117**, 2287.
39 O. Roth and J. A. LaVerne, *J. Phys. Chem. A*, 2011, **115**, 700.
40 S. Sanguanmith, J. Meesungnoen and J.-P. Jay-Gerin, *Chem. Phys. Lett.*, 2013, **588**, 82.
41 Y. Frongillo, T. Goulet, M.-J. Fraser, V. Cobut, J. P. Patau and J.-P. Jay-Gerin, *Radiat. Phys. Chem.*, 1998, **51**, 245.
42 A. Hiroki, S. M. Pimblott and J. A. LaVerne, *J. Phys. Chem. A*, 2002, **106**, 9352.
43 A. J. Elliot and D. M. Bartels, *The reaction set, rate constants and g-values for the simulation of the radiolysis of light water over the range 20 to 350 °C based on information available in 2008*, Report AECL No. 153-127160-450-001, Atomic Energy of Canada Limited, Chalk River, Ontario, Canada, 2009.
44 B. H. J. Bielski, D. E. Cabelli, R. L. Arudi and A. B. Ross, *J. Phys. Chem. Ref. Data*, 1985, **14**, 1041.
45 V. Cobut, Y. Frongillo, J. P. Patau, T. Goulet, M.-J. Fraser and J.-P. Jay-Gerin, *Radiat. Phys. Chem.*, 1998, **51**, 229.
46 J. Meesungnoen, A. Filali-Mouhim, S. Mankhetkorn and J.-P. Jay-Gerin, *J. Phys. Chem. A*, 2001, **105**, 2125.
47 J. Meesungnoen, J.-P. Jay-Gerin, A. Filali-Mouhim and S. Mankhetkorn, *Radiat. Res.*, 2002, **158**, 657.
48 N. Autsavapromporn, J. Meesungnoen, I. Plante and J.-P. Jay-Gerin, *Can. J. Chem.*, 2007, **85**, 214.
49 S. Sanguanmith, Y. Muroya, T. Tippayamontri, J. Meesungnoen, M. Lin, Y. Katsumura and J.-P. Jay-Gerin, *Phys. Chem. Chem. Phys.*, 2011, **13**, 10690.
50 R. Meesat, S. Sanguanmith, J. Meesungnoen, M. Lepage, A. Khalil and J.-P. Jay-Gerin, *Radiat. Res.*, 2012, **177**, 813.
51 M. Tachiya, *Radiat. Phys. Chem.*, 1983, **21**, 167.
52 S. M. Pimblott, M. J. Pilling and N. J. B. Green, *Radiat. Phys. Chem.*, 1991, **37**, 377. See also S. M. Pimblott and N. J. B. Green, in *Research in Chemical Kinetics*, ed. R. G. Compton and G. Hancock, Elsevier, Amsterdam, 1995, vol. 3, p. 117.
53 T. Goulet, M.-J. Fraser, Y. Frongillo and J.-P. Jay-Gerin, *Radiat. Phys. Chem.*, 1998, **51**, 85.
54 I. Plante, Ph.D. thesis, Université de Sherbrooke, Sherbrooke, Québec, Canada, 2009.
55 M. Běgusová and S. M. Pimblott, *Radiat. Prot. Dosim.*, 2002, **99**, 73.
56 T. Tippayamontri, S. Sanguanmith, J. Meesungnoen, G. R. Sunaryo and J.-P. Jay-Gerin, *Recent Res. Dev. Phys. Chem.*, 2009, **10**, 143.
57 *CRC Handbook of Chemistry and Physics*, ed. W. M. Haynes, CRC Press, Boca Raton, Florida, 91st edn, 2010, pp. 5–75.
58 R. E. Weston, Jr and H. A. Schwarz, *Chemical Kinetics*, Prentice-Hall, Englewood Cliffs, New Jersey, 1972.
59 We should note that the use of high-energy protons as primary particles was more appropriate here than that of fast electrons since we wanted to study track segments over which the LET is essentially constant. In fact, a proton that has the same LET as an electron must also have an energy 2000 times larger and, consequently, its LET is much less affected by a given series of energy depositions. See ref. 8, 41 and 45.
60 S. Heinze, T. Stolz, D. Ducret and J.-C. Colson, *Fusion Sci. Technol.*, 2005, **48**, 673 (*Proceedings of the 7th International Conference on Tritium Science and Technology*, Baden Baden, Germany, September 12–17, 2004).
61 B. Pastina and J. A. LaVerne, *J. Phys. Chem. A*, 1999, **103**, 1592.

62 Z. D. Draganić and I. G. Draganić, *J. Phys. Chem.*, 1969, **73**, 2571; Z. D. Draganić and I. G. Draganić, *J. Phys. Chem.*, 1971, **75**, 3950.

63 The product of a solute's (or scavenger's) concentration and its rate constant for reaction with one of the primary radical species is called its "scavenging power", with units of s^{-1}. The inverse of the scavenging power gives a measure of the time scale over which the scavenging is occurring or, on the other hand, the lifetime of the radical with respect to that reaction (see McCracken *et al.*, ref. 17).

64 In fact, Gagnon and Appleby (ref. 22) reported the ratios G/G° of the H_2O_2 yield produced by the tritium β radiation in the presence of the $^{\bullet}OH$ scavenger (Br^{-}) to the yield in its absence. Unfortunately, G°, the value obtained by "extrapolating the yields in bromide solutions to zero Br^{-} concentration", was not given in their paper. We therefore decided to use here for $G^{\circ}(H_2O_2)$, the value of ~0.78 molecule per 100 eV that we calculated for the H_2O_2 yield in the 7.8 keV ^{3}H β-electron radiolysis of pure, air-free water at ~1 μs (see Fig. 4).